# Development of Antibody-Based Fiber-Optic Sensors for Detection of a Benzo[a]pyrene Metabolite

**Bruce J. Tromberg,[1] Michael J. Sepaniak,* and Jean Pierre Alarie**

*Department of Chemistry, University of Tennessee, Knoxville, Tennessee 37996-1600*

**Tuan Vo-Dinh**

*Advanced Monitoring Development Group, Health and Safety Research Division, Oak Ridge National Laboratory, Oak Ridge, Tennessee 37831-6101*

**Regina M. Santella**

*Cancer Institute, Division of Environmental Sciences, Columbia University, New York, New York 10032*

**This paper describes the development of an antibody-based fiber-optic sensor designed to detect benzo[a]pyrene (BP) metabolites, in this case r-7,t-8,9,c-10-tetrahydroxy-7,8,9,10-tetrahydrobenzo[a]pyrene (benzopyrenetetraol or BPT), a naturally fluorescent hydrolysis product of DNA adducts that forms during BP metabolism. The sensor's principle of operation is based on diffusion of BPT into the fiber's reagent phase where it complexes with monoclonal anti-BPT antibody. Reagent phase is immobilized inside a reusable sensing tip. It consists of either membrane-entrapped liquid antibody or antibody immobilized on 7-μm silica beads. The antibody binds and concentrates BPT in the fiber's viewing region until equilibrium with the sample is achieved. Typical measurements are performed in 15 min under nonequilibrium conditions. The 325-nm line of a He:Cd laser provides excitation of the immune complex. The intensity of the resulting fluorescence emission is directly proportional to the amount of BPT in the sample. Sensor response rate varies with BPT concentration in the sample and, under certain circumstances, with antibody concentration in the sensor. At high antibody concentrations, sensor response rate is linear for about 2 h. For 15-min incubations, typical limits of detection are $5 \times 10^{-10}$ M. Significant chemical selectivity is also demonstrated despite the presence of structurally and spectrally similar polynuclear aromatic (PNA) interferents. These results indicate that the fluoroimmunosensor (FIS) is capable of performing highly sensitive and selective immunoassays and could be useful as a screening instrument for BP metabolites in biological samples. Furthermore, the information provided by this work should be generally applicable to the development of devices for chemically similar systems.**

Among the primary considerations involved in the design and development of fiber-optic chemical sensors (FOCSs) are the nature of the reagent-phase/analyte interaction and the detectability of the measured optical property. In view of these circumstances, it is not surprising that a large number of FOCSs have been described that utilize the excellent sensitivity of fluorescence detection in conjunction with the chemical specificity of ligand/binder reactions (*1–3*). The majority of these devices have been used to determine pH (*4, 5*) and to detect ions (*6, 7*) and small molecules, e.g. $CO_2$ (*8, 9*) and $NH_3$ (*10*). The FOCS measurement of large molecules (molecular weight ≥ 200) has been accomplished primarily by incorporating biologically significant ligand/binder reactions into the sensor's reagent phase. Successful examples of these devices include those that exploit enzyme/substrate (*11–13*), lectin/carbohydrate (*14*), antibody/antigen (Ab:An) (*15–18*), and antibody/hapten (Ab:Hn) (*19*) interactions. The versatility of these fiber-optic biosensors is generally a function of the commercial availability (or ease of manufacture) of the required biochemicals and their capacity to be adapted to an appropriate sensor design.

FOCSs that employ immunochemical reagent phases are particularly promising since they have the potential to perform highly sensitive and selective in situ measurements of a broad variety of compounds. Antibodies to an extensive range of materials are commercially available or can be produced. Because they rely upon the outstanding specificity of antibody/antigen recognition, antibody-based FOCSs can be fabricated to detect trace amounts of materials in complex matrices. By use of immunoassays coupled with small-diameter fiber-optic instrumentation, site-specific analytical measurements can be conducted that probe nanoliter to low microliter sample volumes.

The overall sensitivity of FOCSs with immunochemical reagent phases is a dual function of the Ab:An affinity constant ($K_a$) and the sensitivity of the measured optical parameter. Using high-affinity antibody reagent phases and laser-excited fluorescence detection, we have developed fluoroimmunosensors (FISs) that are capable of femtomole limits of detection (*15, 16, 19*). These previously described FIS reagent phases have consisted of roughly a monolayer of immunochemical covalently bound to the fiber's sampling terminus. This approach is useful for competitive binding measurements since, provided there is sufficient material for detectability, assay sensitivity is inversely proportional to the amount of immobilized limiting reagent (*20*). In the case of direct immunoassays of natural fluorophores and antibody "sandwich" assays, however, sensitivity and linearity are directly proportional to the amount and availability of immobilized binder (*20*). Optimum sensor performance can therefore be achieved for these measurements by maximizing reagent phase loadings and binding site orientation.

In this work, an FIS design was required that could perform direct immunoassays of the naturally fluorescent polynuclear aromatic (PNA) compound *r*-7,*t*-8,9,*c*-10-tetrahydroxy-7,8,9,10-tetrahydrobenzo[*a*]pyrene (benzopyrenetetraol or BPT). BPT's significance is derived from the fact that it is a bioindicator of an individual's exposure to the carcinogenic PNA benzo[*a*]pyrene (BP). BP is metabolized in vivo to a specific diol–epoxide derivative of BP, *r*-7,*t*-8-dihydroxy-*t*-9,10-epoxy-7,8,9,10-tetrahydrobenzo[*a*]pyrene (BPDE), which covalently binds to DNA (*21, 22*). The resulting BPDE–DNA adducts are eliminated through urine and feces (*23*). In order to determine the extent of BPDE–DNA adduct formation, weakly fluorescent BPDE–DNA can be converted (via acid

[1] Present address: Beckman Laser Institute and Medical Clinic, 1002 Health Sciences Rd. East, University of California, Irvine, Irvine, CA 92715.

0003-2700/88/0360-1901$01.50/0 

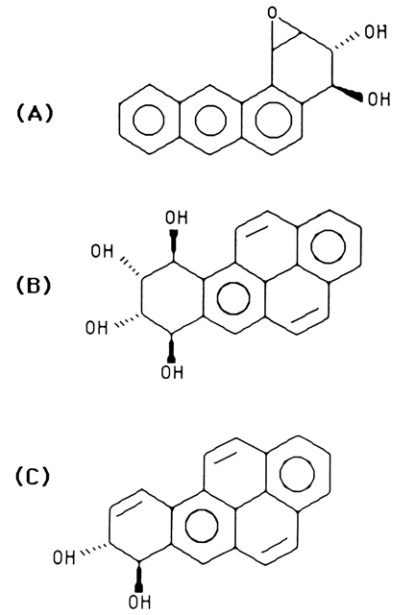


**Figure 1.** Structures of PNA metabolites: (A) 3,4-dihydroxy-1,2-epoxy-1,2,3,4-tetrahydrobenz[*a*]anthracene (benzoanthracenediol epoxide or ADE), (B) *r*-7,*t*-8,9,*c*-10-tetrahydroxy-7,8,9,10-tetrahydrobenzo[*a*]pyrene (benzopyrenetetraol or BPT), and (C) 7,8-dihydroxy-7,8-dihydrobenzo[*a*]pyrene (benzopyrenediol or BPD).

hydrolysis) to the highly fluorescent BPT (*24*). Analysis of BPT in hydrolyzed biological samples is, therefore, evidential of an individual's exposure to benzo[*a*]pyrene (*25*).

In this work, BPT FISs were constructed by using purified monoclonal antibodies immobilized at the end of 200- and 600-$\mu$m core-diameter optical fibers. Because of previously encountered difficulties associated with preparing, handling, and regenerating sensors with reagent phases covalently bound to fibers (*15*), reusable sensing tips capped with highly permeable dialysis membranes were fabricated for this work. Measurements were performed with two types of reagent phases. The first consisted of a high concentration of liquid-phase antibody that was entrapped within a sensing tip. The second was composed of solid-phase antibody immobilized on 7 $\mu$m diameter Protein-A-derivatized silica particles suspended in a sensing tip.

Sensor response was dependent upon analyte (i.e., BPT) diffusion into the sensor where it was concentrated as a result of the formation of an immune complex. The effects of potential interferences could be reduced by removing the sensor from the sample and dialyzing to remove unbound impurities. Data from our investigations are organized in a manner that permits evaluation of the sensor's analytical figures of merit, including linearity, precision, limits of detection, selectivity, and rate of response. FIS performance is further discussed with regard to the practical utility of the device and the influence of the analyte's characteristics on sensor design.

## EXPERIMENTAL SECTION

**Materials.** Due to the fact that PNAs are haptens, i.e., they are too small to elicit an immune response, anti-PNA antibodies must be raised to protein-conjugated PNAs. Accordingly, monoclonal antibody 8E11 was developed from the spleen cells of a mouse immunized with BPDE–guanosine covalently coupled to the protein bovine serum albumin (BSA). In order to isolate the immunoglobin G (IgG) antibody fraction, crude mouse ascites fluid was purified by precipitation with 30% ammonium sulfate. The precipitate was redissolved, dialyzed against phosphate-buffered saline (PBS), pH 7.4, and diluted to 1.5 mg of IgG/mL.

Cross-reactivity studies were performed by using competitive enzyme-linked immunosorbent assay (ELISA). These results have shown that antibody 8E11 recognizes DNA adducts and free BPT with approximately the same high affinity (*26*). In addition, the antibody recognizes BP 7,8 diol and BP 9,10 diol, but not BP itself. A thorough description of antibody production, sensitivity, and specificity has been reported (*27*). The value of $K_a$ for Ab:BPT complex formation in PBS was determined by FIS measurements to be approximately $10^8$ $M^{-1}$.

**Table I. Composition of NBS Spike (SRM 1647)[a]**

| no. | constituent | amount, ng/mL |
|---|---|---|
| 1 | anthracene | 32.9 |
| 2 | benz[*a*]anthracene | 50.3 |
| 3 | benzo[*a*]pyrene | 53.0 |
| 4 | fluoranthene | 101.0 |
| 5 | pyrene | 98.4 |
| 6 | naphthalene | 225.0 |
| 7 | acenaphthylene | 191.0 |
| 8 | acenaphthene | 210.0 |
| 9 | fluorene | 49.2 |
| 10 | phenanthrene | 50.6 |
| 11 | chrysene | 46.8 |
| 12 | benzo[*b*]fluoranthene | 51.1 |
| 13 | benzo[*k*]fluoranthene | 50.2 |
| 14 | benzo[*ghi*]perylene | 40.1 |
| 15 | dibenz[*a*,*h*]anthracene | 36.8 |
| 16 | indeno[1,2,3-*cd*]pyrene | 40.6 |

[a] Spiked sample consisted of $8.9 \times 10^{-8}$ M BPT in Fetal Calf Serum with the listed concentrations of PNAs.

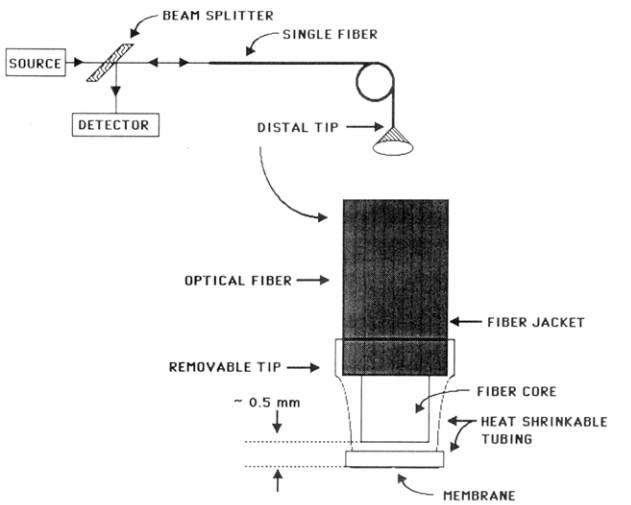


**Figure 2.** Schematic diagram of instrumental apparatus and magnified view of sensing tip.

All PNA haptens were obtained either from the Midwest Research Institute (MRI), Kansas City, MO, or from the National Bureau of Standards (NBS), Gaithersburg, MD. Figure 1 is an illustration of BPT and two structurally similar PNAs used in a series of interference studies. Stock solutions (0.05 mg/mL) of 3,4-dihydroxy-1,2-epoxy-1,2,3,4-tetrahydrobenz[*a*]anthracene (anthracenediol epoxide or ADE, Figure 1a), BPT (Figure 1b), and 7,8-dihydroxy-7,8-dihydrobenzo[*a*]pyrene (BP-diol or BPD, Figure 1c) were prepared in ethanol. Working solutions ranging from $10^{-6}$ to $10^{-10}$ M were made by diluting stock solutions in PBS. Additional interference studies were performed by using a solution that was $8.9 \times 10^{-8}$ M BPT in fetal calf serum (FCS) spiked with 16 PNAs from an NBS standard reference material (SRM 1647). The final concentrations of the 16 PNA interferants in the FCS sample are listed in Table I.

**Apparatus.** A detailed description of the FIS apparatus is provided elsewhere (*15*). The primary components of the instrument used in this study are schematically illustrated in Figure 2. The excitation source consists of an 8-mW Model 4230 Liconix He:Cd laser (Liconix, Inc., Sunnyvale, CA). The 325-nm line of the laser is focused onto the fiber after passing through a 20% T laser line filter (Corion Corp., Holliston, MA), and a beam splitter (a 25 mm diameter mirror with a 1.5 mm diameter hole in the center). Selection of the PNA fluorescence emission is accomplished by using a 40% T 40-nm full width at half maximum

(fwhm) band-pass filter centered at 400 nm (Corion Corp.). The fluorescence emission is detected by a Hamamatsu Model R760 photomultiplier tube operated at −1000 V dc. The output of a Keithly Model 485 picoammeter (Keithly Instruments, Inc., Cleveland, OH) used to process the photocurrent is displayed on a strip chart recorder. A Uniblitz Model SD-10 shutter (Vincent Associates, Rochester, NY) is programmed to open for 1 s every 90 s in order to provide semicontinuous, controlled-duration laser excitation. This allows observation of immune-complex formation in near-real time and helps minimize photothermal/photochemical effects.

**Sensor Fabrication.** Sensors were constructed from either 200-μm or 600-μm core-diameter plastic-clad, multimode, fused silica fibers (General Fiber Optics, Cedar Grove, NJ). Our previously reported FIS designs utilized separate reagent-bonded fibers for each measurement (*15*, *16*, *19*). In this study, a single 1 m long fiber remained dedicated to the instrument and each analysis was performed with a reusable sensing tip (illustrated in Figure 2). Tips were fabricated by tapering heat-shrink tubing around the fiber's jacket and core. Very high permeability cellulose dialysis membrane (reference no. 10.17, Diachema AG, Zurich, Switzerland; thickness, 7 μm; molecular weight cutoff, 10 000) was stretched across the face of the tip and positioned with another piece of heat-shrink tubing roughly 0.5 mm from the fiber's face. When assembled, a seal was formed between the fiber jacket and the tubing. Each tip could easily be slipped off the fiber to be refilled with fresh reagent phase.

Two types of reagent phases were employed. The first consisted of $10^{-6}$–$10^{-8}$ M liquid-phase antibody (molecular weight 160 000) solutions entrapped behind the sensing tip's 10 000 molecular-weight-cutoff membrane. All liquid-phase sensors were constructed with 200 μm diameter fibers. Total sensor volume for these devices was approximately 20–40 nL, resulting in roughly 3–4 ng of immobilized antibody.

The second type of reagent phase was composed of antibody immobilized on silica beads suspended in a sensing tip. Durasphere silica particles (7-μm diameter, 500-Å pore size) were purchased from the manufacturer (Alltech, Inc., Deerfield, IL) with covalently bound Protein A. Reagent phase was prepared by incubating, overnight, 100 μL of 1.5 mg antibody/mL (in PBS, pH 7.4) with 12 mg (dry weight) of beads. The noncovalent antibody/Protein A linkage was selected due to its excellent stability ($K_a$ for Ab:Protein A complex formation $\approx 10^6$), simplicity, and binding site orientation. Protein A is known to specifically bind the Fc or "tail" portion of the antibody molecule, thus leaving the antibody's binding sites available to interact with antigen (*28*). The bead binding capacity was determined to be roughly 1.9 mg of antibody/g. Sensor tips containing solid-phase antibodies were assembled on 600 μm diameter fibers. The bead density was adjusted to 16.6 mg/mL in order to minimize optical problems associated with settling and scattering. Tip volume was approximately 140 nL, resulting in a total amount of immobilized antibody (4.2 ng) that was comparable with liquid-phase sensors.

**Measurements.** All FIS assays were performed either in a sequential, stepwise, or pseudocontinuous fashion. Sequential analyses were implemented by filling the sensing tip with a constant concentration of fresh antibody prior to each measurement. Measurements were completed by incubating sensors for a specified interval (typically 15 min for liquid-phase and 45 min for solid-phase tips) in 1-mL stirred solutions. During this period, materials that were permeable to the membrane diffused into the reagent phase and became conjugated with their specific antibody. Following incubation, the sensor was rinsed in PBS for at least 4.5 min. During rinsing, unbound interferents were dialyzed out of the sensing tip leaving only antibody-bound material confined to the fiber's viewing region. Signal levels were obtained from the difference between pre- and postincubation signal-to-noise ratios (S/N) acquired while the sensor was in PBS.

Stepwise data collection procedures took advantage of the large amount of unbound antibody that remained in the sensor following each short incubation. Measurements were performed by loading the tip with excess antibody and incubating the FIS for a specified interval (typically 15 min) in several samples. The FIS was re-zeroed prior to each analysis by allowing the PBS rinse signal from the previous measurement to serve as the base line for the next determination. As with sequential measurements, difference information was used to record signal levels.

Pseudocontinuous operation was achieved by observing concentration-dependent changes in S/N without rinsing in PBS. Because of antibody binding, the sensor's response to BPT continued to increase until equilibrium was achieved (approximately 12 h). S/N values were calculated for stepwise, sequential, and pseudocontinuous analyses by using peak-to-peak noise levels obtained during measurements of blank PBS solutions.

In order to confirm the concentrating effect of immune-complex formation, blank measurements were conducted that utilized nonspecific protein reagents. Liquid-phase blank sensors were loaded with 1.5 mg of rabbit IgG/mL of PBS (Cooper Biomedical, Inc., Malvern, PA). Solid-phase devices contained 16.6 mg of Protein A beads/mL of PBS. Sensors were incubated in several different concentrations of BPT using stepwise and sequential procedures. FIS response increased until signal levels reached those obtained during bare-fiber measurements (about 15 min), after which no further elevations in signal were observed. PBS rinses of blank sensors caused the FIS signal to return to base line within 3 minutes, indicating negligible nonspecific binding effects.

## RESULTS AND DISCUSSION

The FISs described in this work were designed to perform sensitive, low-volume assays of naturally fluorescent bioindicators of benzo[*a*]pyrene–DNA adducts. Although applications of this device are limited to in vitro analyses of BPT in hydrolyzed biological samples, FIS performance characteristics indicate that it is capable of functioning in a variety of matrices with comparable or superior speed, sensitivity, and/or selectivity to established techniques (*25*, *29*–*34*). Of equal importance is the fact that this study validates the sensor's principles of operation. With the FIS's fundamental response features defined, similarly constructed devices could be used for in vivo analyses of chemically analogous systems.

In order to determine which factors influence FIS performance, dose-response data were obtained for BPT solutions under a variety of conditions. Among the parameters examined were the sensor's time-dependent concentrating effect, its ability to discriminate between analyte and interferences, and the consequence of variations in BPT and antibody concentration on FIS response. Results from these investigations are used to evaluate the sensor's analytical figures of merit. Accordingly, the ensuing discussion focuses on FIS linearity, limits of detection, precision, response kinetics, and selectivity.

**Linearity.** The sensor's temporal behavior was examined for approximately 12 h in order to determine the period of time over which the FIS was capable of a linear response. Conditions for the time-dependent study, illustrated in Figure 3, consisted of either $1.9 \times 10^{-6}$ M liquid-phase or $1.9 \times 10^{-7}$ M solid-phase antibody loaded in the sensing tip. The liquid reagent-phase sensor was incubated in $1.6 \times 10^{-8}$ M BPT and the solid-phase device was placed in $1.6 \times 10^{-7}$ M solutions.

In contrast to blank sensors, antibody-filled FIS signals continued to rise over the entire measurement period. S/N levels were greater for the solid-phase assay (Figure 3b) because the solid-phase device utilized a larger diameter fiber and probed a more concentrated solution. The linear response period was about the same for both sensors, extending for roughly 2 h.

The "concentrating factor" for each sensor was determined by comparing antibody-filled FIS signals with those obtained from blank sensors incubated in the same BPT solutions. These results, listed in Table II, indicate that the liquid-phase device was capable of nearly a factor of 2 greater concentrating effect. At 300 min the solid-phase S/N ratio was 20 times the blank level and the sensor had appeared to reach equilibrium. In contrast, the 300-min liquid-phase S/N ratio was roughly 40 times greater than the blank's and the response continued to increase for nearly 6 h more.

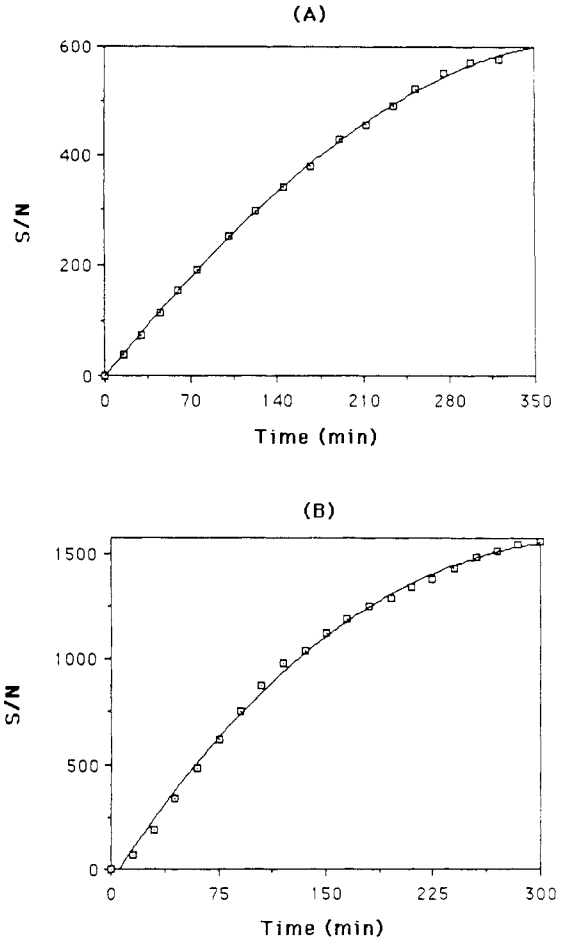


**Figure 3.** FIS temporal response: S/N vs time for (A) liquid antibody reagent-phase sensor in $1.6 \times 10^{-8}$ M BPT and (B) bead-immobilized antibody reagent-phase sensor in $1.6 \times 10^{-7}$ M BPT.

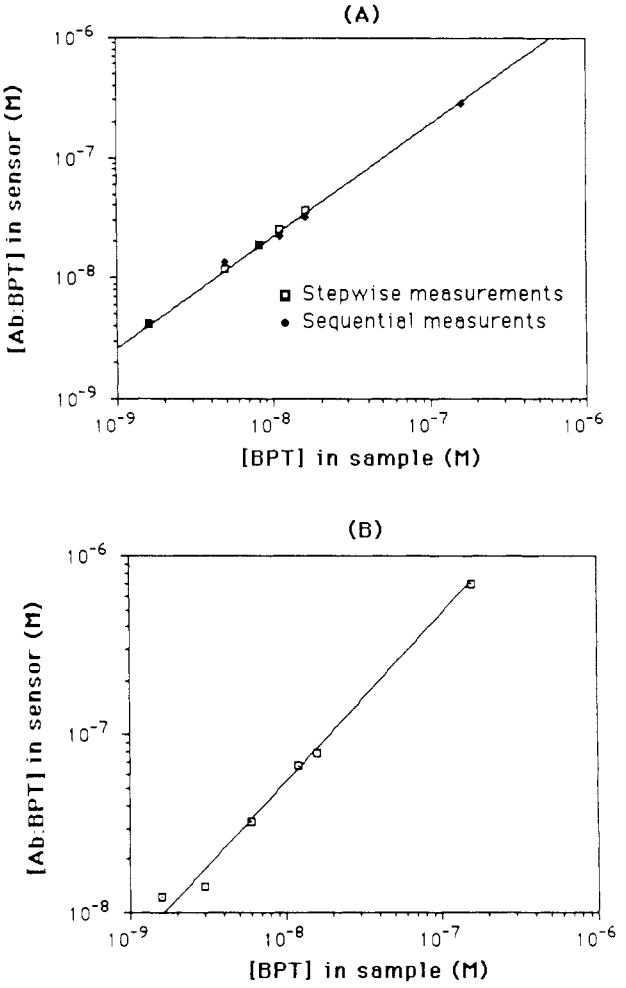


**Figure 4.** FIS dose response: [Ab:BPT] vs [BPT] for (A) liquid antibody reagent-phase sensors, 15-min incubations, and (B) bead-immobilized antibody reagent-phase sensors, 45-min incubations.

**Table II. Time-Dependent Concentrating Factors**

| time, min | concentrating factor: liquid reagent phase | concentrating factor: bead reagent phase |
|---|---|---|
| 15 | 2.6 | 0.9 |
| 30 | 5.0 | 2.5 |
| 45 | 7.8 | 4.4 |
| 75 | 13.2 | 8.1 |
| 120 | 20.5 | 12.7 |
| 165 | 25.9 | 15.5 |
| 255 | 35.7 | 19.3 |
| 300 | 39.1 | 20.3 |

The time ($t$) for each sensor to reach equilibrium was determined by performing a least-squares, third-order polynomial regression fit on the temporal response data. The equations for the liquid and bead sensors are, respectively

$$S/N = 11.70 + 2.705t - 0.002t^2 \quad (1)$$

$$S/N = -67.72 + 10.81t - 0.022t^2 + (1.17 \times 10^{-5})t^3 \quad (2)$$

Setting $d(S/N)/dt = 0$ in each case yields $t_{(\text{equilibrium-liquid})} = 11$ h and $t_{(\text{equilibrium-bead})} = 5$ h. These results indicate that the FIS is capable of responding linearly (and nonlinearly) for long periods of time. The actual working range is probably a function of the relative concentrations of antibody and hapten, the $K_a$, and the occurrence of fluorescence inner-filter effects. Inequalities in one or more of these factors may, therefore, have accounted for the bead sensor's reduced dynamic range.

Temporal response data can also be used to provide fundamental information including the $K_a$ and the concentration of antibody binder in the sensing tip. Substituting $t_{(\text{equilibrium})} \approx 11$ h into eq 1 yields $S/N_{(\text{equilibrium})} = 930$. Because of the fact that free [BPT] $\ll$ [Ab:BPT], virtually all of the observed equilibrium signal was contributed by Ab:BPT. As a result, using independently obtained calibration data, $S/N = 930$ corresponded to [Ab:BPT] $\approx 1 \times 10^{-6}$ M. Since the initial free [Ab] was $1.9 \times 10^{-6}$ M, the final free equilibrium [Ab] was roughly $9 \times 10^{-7}$ M. Furthermore, neglecting membrane adsorption and polarization effects, the free equilibrium [BPT] inside the sensor was approximately equal to the [BPT] in the sample. Substituting these values into the equilibrium expression for Ab:BPT formation

$$K_a = [\text{Ab:BPT}]/([\text{Ab}][\text{BPT}]) \quad (3)$$

yields $K_a \approx 8 \times 10^7$ M$^{-1}$. During long incubations, our experiments indicate that membrane adsorption and polarization may actually have occurred. Accordingly, the exact value for free [BPT] inside the sensor was probably less than $1.6 \times 10^{-8}$ M and the $K_a$ may have been slightly larger than estimated. In principle, this FIS-derived determination of the formation constant is equivalent to the well-established equilibrium dialysis technique (*35*).

Alternately, when the $K_a$ is known through independent experiments, the concentration of free antibody in the sensing tip can be derived from temporal response data and eq 3. If the initial free [Ab] is unknown, it can then be deduced from the sum of bound and free components.

Concentration-dependent linearity was evaluated by obtaining the dose-response data illustrated in Figure 4. Sensors were loaded with a constant amount of antibody and incubated for either 15 (liquid tips) or 45 min (bead tips) in varying

concentrations of BPT. These incubation times were selected because temporal response data indicated they were of sufficient duration to observe approximately a factor of 2 concentrating effect. The [Ab:BPT] values appearing in Figure 4 were obtained by correlating sensor S/N levels to those obtained from bare-fiber Ab:BPT calibration plots.

Liquid-phase sensors were used to perform stepwise and sequential measurements (Figure 4a). The average absolute difference between data obtained with both procedures was 10.5 ± 8.9%. A linear response was observed for up to 2 h without changing reagent phases during stepwise measurements. Sensor response was independent of the measurement sequence of antigen solutions (i.e., signals obtained going from high to low concentrations were the same as those obtained going from low to high). This relatively long stepwise sensor lifetime was consistent with the FIS's previously observed time-dependent linearity. Bead-sensor assays were conducted sequentially (Figure 4b).

As illustrated in parts a and b of Figure 4, the linear response region for sensors using either type of reagent phase extends over approximately 2 decades. The slope, d[Ab:BPT]/d[BPT], is the antibody concentrating effect observed for each assay. Values of 1.8 and 4.3 were derived from the slopes of liquid and bead sensor calibration plots, respectively. These concentrating factors agree reasonably well with those reported at the 15- and 45-min marks of the liquid and bead temporal studies (Table II). This agreement is particularly encouraging since calibration and temporal studies were performed on different days under slightly different instrumental and experimental conditions.

Dynamic range can be extended, at low and high [BPT], by manipulating incubation times. At high [BPT], further extensions in dynamic range should occur by increasing [Ab]. In fact, antibody immobilization on beads was pursued in an effort to elevate its effective concentration beyond liquid-phase levels. Unfortunately, the Protein A beads used in this study did not produce the desired increase in [Ab].

**Limits of Detection.** FIS limits of detection (LOD) are dependent upon assay incubation times, the antibody–hapten association constant ($K_a$), and the sensitivity of the measured optical parameter. In this work, $K_a$ was determined to be $8 \times 10^7$ $M^{-1}$, the minimum detectable [Ab:BPT] for fiber measurements was approximately $1 \times 10^{-9}$ M, and [Ab] for typical liquid-phase assays was $2 \times 10^{-6}$ M. Substitution of these values into eq 3 yields $[BPT] = 6 \times 10^{-12}$ M. This figure represents the minimum concentration of unbound BPT inside the sensor that will yield a detectable equilibrium concentration of Ab:BPT. When the FIS is at equilibrium with regard to the sample, $[BPT]_{(inside)} = [BPT]_{(outside)}$, and $6 \times 10^{-12}$ M also represents the lowest concentration of BPT that can be detected in the sample.

Estimation of sample detection limits can be further understood by considering the effect of dropping sample BPT concentration below $6 \times 10^{-12}$ M. Under these conditions, $[BPT]_{(inside)}$ values are reduced. Substituting smaller $[BPT]_{(inside)}$ levels into eq 3 yields Ab:BPT concentrations that are below the fiber's limit of detection (LOD). Therefore, under the above equilibrium conditions, $[BPT]_{LOD} = 6 \times 10^{-12}$ M. Lower detection limits can be achieved by improving instrumental sensitivity, increasing [Ab], or using higher affinity antibodies. These extremely low detection limits are not, however, encountered in practical FIS applications due to the prohibitively long incubation times required to reach equilibrium. In addition, at long incubation times, the appearance of membrane adsorption and polarization effects would cause $[BPT]_{(inside)} < [BPT]_{(outside)}$. As a result, the observed BPT detection limits would be slightly higher than $6 \times 10^{-12}$ M since greater $[BPT]_{(outside)}$ levels would be required in order to maintain sufficient $[BPT]_{(inside)}$ for Ab:BPT detectability.

In the case of nonequilibrium FIS measurements, LOD can be derived from the sensor's time-dependent concentrating effect and the bare-fiber detectability of Ab:BPT. For 15-min liquid-phase sensor measurements, a concentrating factor of 2 was observed. Consequently, $[BPT]_{(bulk)}$ levels as low as $5 \times 10^{-10}$ M can be probed in order to satisfy the $1 \times 10^{-9}$ M minimum [Ab:BPT] detectability requirement. LOD for 45-min bead sensor incubations (based on a factor of 4 concentrating effect) were $2.5 \times 10^{-10}$ M. Further reductions in FIS detection limits can be achieved by increasing incubation times, though the merits of this approach must be evaluated by weighing the benefits of lower LOD against the disadvantages of longer analysis times. Additional LOD modifications can be affected by altering the sensor's fundamental response parameters.

An experiment designed to illustrate the FIS's excellent low-volume sensitivity was conducted in a 5-μL droplet of $1.6 \times 10^{-9}$ M BPT. Results indicate that BPT was easily detected ($S/N = 39$) after a 30-min incubation. In contrast, bare-fiber FIS measurements yielded a S/N that was close to the detection limit. The large response observed during the 30-min incubation was partly due to solvent evaporation, which increased the BPT concentration and the rate of diffusion into the sensor. Nevertheless, the absolute amount of BPT in the sample was 8 fmol, indicating that the absolute LOD for BPT is in the attomole ($10^{-18}$ mol) region even when relatively short incubations are employed.

**Precision.** FIS precision was evaluated by performing multiple assays of identical BPT solutions. In a series of five, 45 min long, bead-sensor sequential measurements of $3 \times 10^{-9}$ M BPT, the average S/N was 13.85 ± 0.86. The 6.2% relative standard deviation (RSD) displayed by these sequential bead-sensor assays was approximately the same as the RSD encountered during sequential liquid-phase measurements. Stepwise analyses, however, were nearly 2.5 times less reproducible, exhibiting a 15% RSD. Membrane memory effects may have been responsible for this discrepancy since the sensing tips were thoroughly washed (inside and out) between sequential assays while stepwise rinses consisted of a brief exposure to PBS dialysis solutions.

Additional factors which may contribute to imprecision include variations in instrumental response and irreproducible measurement conditions. Fluctuations in the latter, particularly rate of analyte mass transport, can be extremely deleterious when highly sensitive, nonequilibrium assays are performed. Reproducing in situ conditions is relatively straightforward for benchtop measurements. It is, however, a critically important challenge that must be addressed before the FIS can provide accurate information from in vivo samples.

**Response Kinetics.** FIS response can be described by a two-step mechanism involving (1) transport of BPT across the membrane into the reagent phase and (2) reaction of BPT with antibody to form Ab:BPT. Step 1 is represented by

$$BPT_{outside} \underset{k_{-d}}{\overset{k_d}{\rightleftharpoons}} BPT_{inside} \qquad (4)$$

The rate constants $k_d$ and $k_{-d}$ for this relatively slow process are a function of BPT's diffusion through the membrane material. In step 2

$$BPT_{inside} + Ab_{inside} \underset{k_{-1}}{\overset{k_1}{\rightleftharpoons}} Ab{:}BPT_{inside} \qquad (5)$$

the rate constants $k_1$ (typically $10^7$–$10^9$ $M^{-1}$ $s^{-1}$) and $k_{-1}$ (typically $10^2$–$10^4$ $s^{-1}$) are responsible for the rapid rate of immune complex formation inside the reagent phase (*36*, *37*). At high $[Ab]_{inside}$, the rate of BPT diffusion in the reagent phase does not significantly influence liquid and bead-sensor

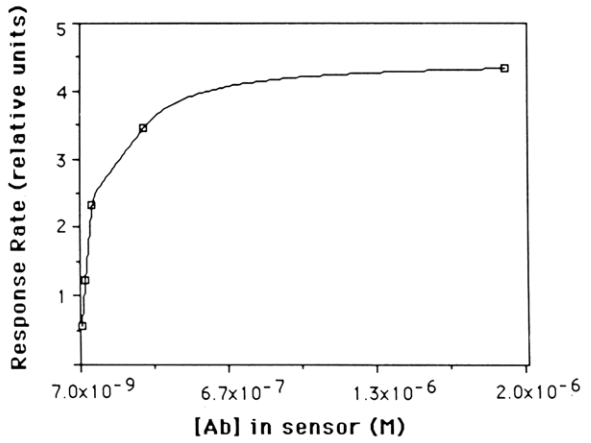


**Figure 5.** FIS response rate (change in S/N during 15-min incubations) as a function of sensor [Ab] for liquid antibody reagent-phase sensors.

response, though it may be important in determining the response rate for gel or polymer-based devices.

Since $BPT_{inside}$ is a rapidly reacting intermediate whose time-dependent concentration, $d[BPT]_i/dt$, is approximately zero, the entire kinetic scheme can be simplified by applying the steady-state approximation to eq 4 and 5. By assuming that $k_1$ is much greater than $k_{-1}$, the rate of Ab:BPT formation becomes

$$d[Ab:BPT]/dt \approx k_1 k_d [Ab]_i [BPT]_o / (k_{-d} + k_1 [Ab]_i) \quad (6)$$

where the subscripts "i" and "o" represent "inside" and "outside" the sensing tip. When $[Ab]_i$ is large, eq 6 reduces to

$$d[Ab:BPT]/dt \approx k_d [BPT]_o \quad (7)$$

and sensor response rate is simply a function of the external analyte concentration and the rate constant for its diffusion across the membrane.

Figure 5 summarizes sensor behavior by illustrating the influence of $[Ab]_i$ (at constant $[BPT]_o$) on response rate. At high $[Ab]_i$, sensor response rate is nearly independent of antibody concentration. In this region, antibody binder is in excess. Sensor response kinetics can be described by eq 7, and small perturbations in $[Ab]_i$ have little or no influence on response rate.

In contrast, at sufficiently low antibody concentrations $k_{-d} \gg k_1[Ab]_i$ and eq 6 reduces to

$$d[Ab:BPT]/dt \approx k_1 k_d / k_{-d} [Ab]_i [BPT]_o \quad (8)$$

In this case, sensor response kinetics are probably second order. These conditions are represented by the steep portion of Figure 5. In this low $[Ab]_i$ region, small changes in $[Ab]_i$ produce large variations in response rate. Since it is not desirable to operate the FIS under these rapidly changing conditions, a high concentration of Ab should be maintained inside the sensor for most applications.

When $[Ab]_i$ is large, a plot of the change in response over a 15-min interval ($d[Ab:BPT]/dt$) vs $[BPT]_o$ should yield a straight line whose slope, $k_d$, is the rate constant described in eq 7. Calibration data are redisplayed in parts a and b of Figure 6 to illustrate this relationship. For liquid reagent phases (Figure 6a) $k_d = 2.5 \times 10^{-3}$ s$^{-1}$. When bead reagent phases are employed, $k_d = 1.6 \times 10^{-3}$ s$^{-1}$ (Figure 6b). The agreement between liquid and bead rate constants is reasonable, though the slightly slower bead kinetics may be attributable to the presence of solid particles interfering with membrane transport. It should be noted that rinsing times were short (4.5 min) relative to the time required to achieve a concentrating factor of one, indicating that $k_{-d} > k_d$, perhaps due to a slight pressure differential between the "closed" 20-nL

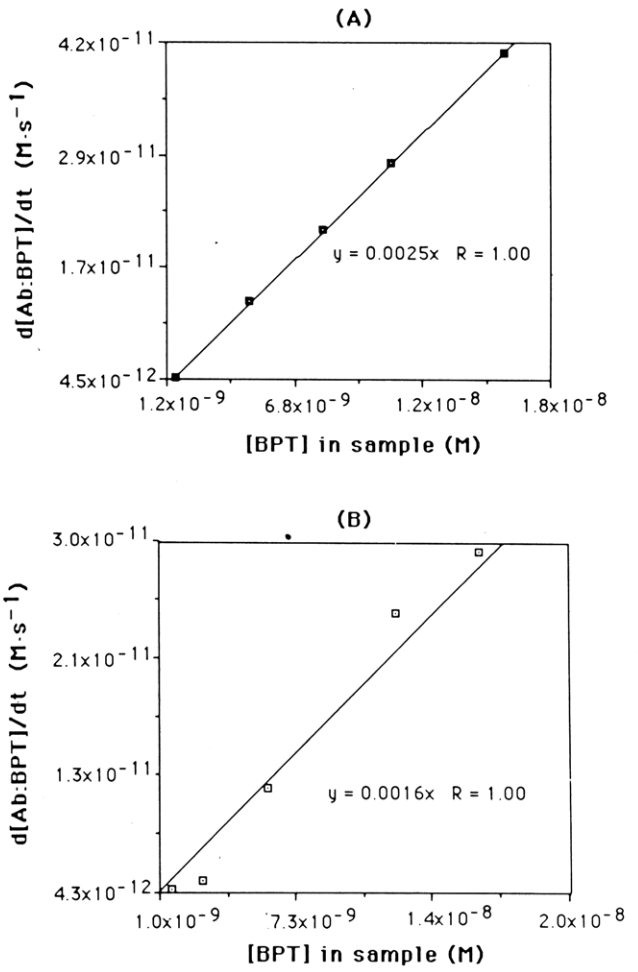


**Figure 6.** FIS response rate as a function of sample [BPT] for (A) liquid antibody reagent-phase sensors, 15-min incubations, and (B) bead-immobilized antibody reagent-phase sensors, 45-min incubations.

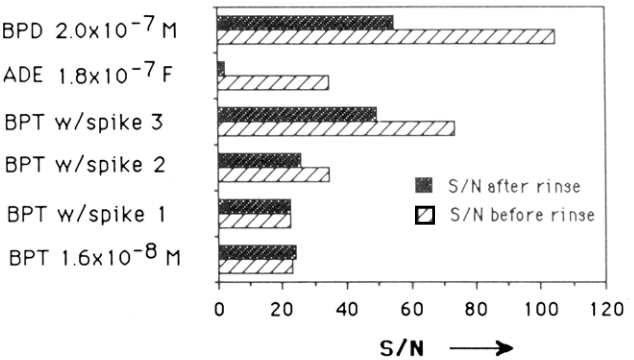


**Figure 7.** FIS interference study in PBS for liquid antibody reagent-phase sensors, 15-min incubations, 4.5-min rinses. All samples contained $1.6 \times 10^{-8}$ M BPT. Spike contents were (1) $1.8 \times 10^{-8}$ F ADE, (2) $1.9 \times 10^{-6}$ F ADE, (3) $1.9 \times 10^{-6}$ F ADE, and $4.0 \times 10^{-8}$ M BPD.

sensor and the open 1-mL sample.

The FIS-derived response constant can also be used to calculate sensor detection limits for any incubation time, "$t$". Integration of eq 7 as a function of time yields, for sequential measurements

$$[Ab:BPT]_t = k_d t [BPT]_o \quad (9)$$

If $k_d$ and the minimum detectable [Ab:BPT] are known, eq 9 can be used as a general expression to provide time-dependent $[BPT]_{LOD}$. Detection limits calculated in this manner are only valid when [Ab] is in excess.

**Selectivity.** Figure 7 summarizes the results of an interference study, performed in PBS, using the PNA interferents

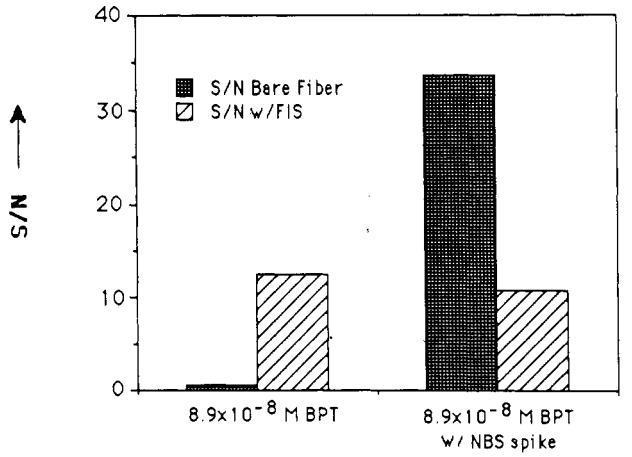


**Figure 8.** FIS interference study in fetal calf serum (FCS) for liquid antibody reagent-phase sensor, 15-min incubation, 4.5-min FCS rinse.

illustrated in Figure 1. Analyses were conducted by incubating liquid reagent-phase sensors for 15-min in BPT and BPT plus PNA solutions. Signal levels observed prior to rinsing were generally greater than those observed following a 4.5-min rinse. These elevated prerinse signals were indicative of the extent of spectral interference provided by the ADE and BPD interferents. In the case of two-component BPT/ADE mixtures (spikes 1 and 2), postrinse FIS signals returned to those obtained for pure BPT solutions, despite the 2 order of magnitude ADE excess in spike 2. These results were not surprising since, as the data in Figure 7 illustrate, pure $1.8 \times 10^{-7}$ F ADE was poorly retained by antibody. The formal analytical concentration is reported since, with time, aqueous ADE hydrolyzes to anthracenetetraol. The exact molar concentration of ADE was therefore not known.

In the case of the three-component BPT/BPD/ADE mixture, postrinse signals dropped precipitously from prerinse levels. The observed signal reduction was probably due primarily to the loss of unbound ADE from the sensor, though the disappearance of unbound BPD may also have contributed to this effect. It is likely that the latter phenomenon occurred to a lesser extent since, as indicated by the pure BPD measurement, significant antibody:BPD binding was observed.

Additional interference studies were carried out in a biological matrix, fetal calf serum (FCS). As illustrated in Figure 8, measurements were performed in spiked and unspiked $8.9 \times 10^{-8}$ M BPT/FCS. The spike was composed of 16 PNA interferents from NBS SRM 1647. Final spike concentrations are listed in Table I. Both bare-fiber and liquid-phase FIS analyses were conducted. FIS rinses were performed in pure FCS. The bare-fiber measurement revealed that, at the excitation and emission wavelengths used in this work, SRM 1647 was responsible for significant spectral interference. The postrinse FIS S/N ratios for spiked and unspiked solutions, however, were 10.5 and 11.5, respectively, indicating that the FIS was capable of excellent chemical selectivity. The sensor was also observed to display slightly diminished sensitivity, probably due to FCS-related elevations in optical background.

The specificity of antibody/hapten interactions is not the sole parameter that determines the sensor's ability to discriminate between structural interferents. Additional selectivity factors include the membrane's molecular-weight cutoff, thickness, and analyte compatibility, as well as the solubility of the analyte in the sensor's reagent phase. In the case of SRM 1647 measurements, a number of hydrophobic components may not have crossed the hydrophilic membrane material. Overall performance was, therefore, probably attributable to the simultaneous action of more than one selectivity determinant.

In conclusion, our results demonstrate that small, hydrophilic, fluorescent haptens can be reliably detected by using membrane-entrapped antibody reagents. Rapid, nonequilibrium measurements can be conducted for long periods of time, provided there is sufficient excess antibody in the sensing tip. An additional unique feature of the FIS is its ability to perform measurements in complex biological matrices.

Data obtained during FIS analyses can be used to characterize sensor response as well as provide fundamental immunochemical information. Improvements in sensor performance can be achieved by optimizing parameters that influence detectability. Among the potential drawbacks to these devices are membrane-related difficulties including memory effects and response-limiting trans-membrane diffusion. Memory effects can be addressed by improved rinsing, however additional impediments to sensor precision may arise if mass transport conditions and incubation times are not precisely reproduced. Despite these obstacles, it is expected that the FIS's outstanding sensitivity, selectivity, and simplicity will encourage further applications and design refinements so that increasingly versatile sensors can be constructed.

## ACKNOWLEDGMENT

The authors wish to thank Rudolf Seitz of the University of New Hampshire for recommending the very high permeability dialysis membrane used in this work.

**Registry No.** BPT, 61490-66-2.

## LITERATURE CITED

(1) Seitz, W. R. *Anal. Chem.* **1984**, *56*, 16A.
(2) Wolfbeis, O. S. *TrAC, Trends Anal. Chem.* **1985**, *4*, 184.
(3) Leiner, M. J. P.; Posch, H. E.; Sharma, A.; Wolfbeis, O. S. In *Optical Fibers in Medicine III*; Katzir, A., Ed.; Proc. SPIE 906-08, Los Angeles, 1988; in press.
(4) Munkholm, C.; Walt, D. R.; Milanovich, F. P.; Klainer, S. M. *Anal. Chem.* **1986**, *58*, 1427.
(5) Peterson, J. I.; Goldstein, S. R.; Fitzgerald, R. V.; Buckhold, D. K. *Anal. Chem.* **1980**, *52*, 864.
(6) Saari, L. A.; Seitz, W. R. *Anal. Chem.* **1983**, *55*, 667.
(7) Wyatt, W. A.; Bright, F. V.; Hieftje, G. M. *Anal. Chem.* **1987**, *59*, 2272.
(8) Gehrich, J. L.; Luebbers, D. W.; Optiz, N.; Hansmann, D. R.; Miller, W. W.; Tusa, J. K.; Yafuso, M. *IEEE Trans. Biomed. Eng.* **1986**, *33*, 117.
(9) Hirschfeld, T.; Miller, F.; Thomas, S.; Miller, H.; Milanovich, F.; Gaver, R. W. *IEEE J. Lightwave Tech.* **1987**, *5*, 1027.
(10) Wolfbeis, O. S.; Posch, H. E. *Anal. Chim. Acta* **1984**, *160*, 305.
(11) Arnold, M. A. *Anal. Chem.* **1985**, *57*, 565.
(12) Kulp, T. J.; Camins, I.; Angel, S. M.; Munkholm, C.; Walt, D. R. *Anal. Chem.* **1987**, *59*, 2849.
(13) Fuh, M. S.; Burgess, L. W.; Christian, G. D. *Anal. Chem.* **1988**, *60*, 433.
(14) Schultz, J. S.; Mansouri, S.; Goldstein, I. J. *Diabetes Care* **1982**, *5*, 245.
(15) Tromberg, B. J.; Sepaniak, M. J.; Vo-Dinh, T.; Griffin, G. D. *Anal. Chem.* **1987**, *59*, 1226.
(16) Petrea, R. D.; Sepaniak, M. J.; Vo-Dinh, T. *Talanta* **1988**, *35*, 139.
(17) Sutherland, R.; Dahne, C.; Place, J. F.; Ringrose, A. S. *Clin. Chem. (Winston-Salem, N.C.)* **1984**, *30*, 1533.
(18) Andrade, J. D.; Vanwagenen, R. A.; Gregonis, D. E.; Newby, K.; Lin, J.-N. *IEEE Trans. Electron Devices* **1985**, *32*, 1175.
(19) Vo-Dinh, T.; Tromberg, B. J.; Griffin, G. D.; Ambrose, K. R.; Sepaniak, M. J.; Gardenhire, E. M. *Appl. Spectrosc.* **1987**, *41*, 735.
(20) Dakubu, S.; Ekins, R.; Jackson, T.; Marshall, N. J. In *Practical Immunoassay: The State of the Art*; Butt, W. R., Ed.; Marcel Dekker: New York, 1984; Chapter 4.
(21) *Environmental Carcinogens: Polycyclic Aromatic Hydrocarbons*; Grimmer, G., Ed.; CRC Press: Boca Raton, FL, 1983.
(22) Brown, H. S.; Jeffrey, A. M.; Weinstein, I. B. *Cancer Res.* **1979**, *39*, 1673.
(23) Kotin, P.; Falk, H. L.; Busser, R. *J. Natl. Cancer Inst.* **1979**, *23*, 541.
(24) Rahn, R. O.; Chang, S. S.; Holland, J. M.; Shugart, L. R. *Biochem. Biophys. Res. Commun.* **1982**, *109*, 262.
(25) Vo-Dinh, T.; Uziel, M. *Anal. Chem.* **1987**, *59*, 1093.
(26) Santella, R. M.; Lin, C. D.; Cleveland, W. L.; Winstein, I. B. *Carcinogenisis* **1984**, *5*, 373.
(27) Santella, R. M.; Lin, C. D.; Dharmaraja, N. *Carcinogenisis* **1985**, *7*, 441.
(28) Forsgren, A.; Sjoquist, J. *J. Immunol.* **1966**, *97*, 822.
(29) Burlingame, A. L.; Straub, K.; Baillie, T. A. *Mass Spectrom. Rev.* **1983**, *2*, 331.
(30) Rahn, R. O.; Chang, S. S.; Holland, J. M.; Stephan, T. J.; Smith, L. H. *J. Biochem. Biophys. Methods* **1980**, *33*, 285.
(31) Vo-Dinh, T. In *Modern Fluorescence Spectroscopy*; Wehry, E., Ed.; Plenum: New York, 1981; Vol. 4, pp 167–192.

(32) Sanders, M. J.; Cooper, R. S.; Small, G. J.; Heisig, V.; Jeffrey, A. M. *Anal. Chem.* **1985**, *57*, 1148.
(33) Randerath, E.; Reddy, M. V.; Gupta, R. C. *Proc. Natl. Acad. Sci. U. S.A.* **1981**, *78*, 6126.
(34) Harris, C. C.; Yolker, R. H.; Hsu, I. C. *Proc. Natl. Acad. Sci. U.S.A.* **1979**, *76*, 5336.
(35) Day, E. D. In *Advanced Immunochemistry*; Williams and Wilkins: Baltimore, MD, 1972.
(36) Pecht, I. In *The Antigens*; Sela, M., Ed.; Academic: New York, 1982; Vol. 6, pp 1-68.
(37) Nisonoff, A.; Hopper, J. E.; Spring, S. B. *The Antibody Molecule*; Academic: New York, 1975; Chapter 2.

RECEIVED for review February 18, 1988. Accepted April 25, 1988. This research was supported by the National Institutes of Health under Contract GM 34730 with the University of Tennessee, Knoxville, and the Office of Health and Environmental Research, U.S. Department of Energy, under Contract DE-AC05-840R21400 with Martin Marietta Energy Systems, Inc. B.J.T. acknowledges support from the U.S. Department of Energy/Oak Ridge Associated Universities predoctoral fellowship program administered at Oak Ridge National Laboratory. R.M.S. acknowledges support from NIH and NIEHS under Contract CA 21111 and ES03881, respectively.

# Fourier Transform Infrared Spectra of Organic Compounds in Solution and as Thin Layers Obtained by Using an Attenuated Total Internal Reflectance Fiber-Optic Cell

**Shimon Simhony and Abraham Katzir**

*School of Physics and Astronomy, Sackler Faculty of Exact Sciences, Tel-Aviv University, Ramat-Aviv, Tel-Aviv 69978, Israel*

**Edward M. Kosower***

*Biophysical Organic Chemistry Unit, School of Chemistry, Sackler Faculty of Exact Sciences, Tel-Aviv University, Ramat-Aviv, Tel-Aviv 69978, Israel*

**A cell lined with Teflon fluorocarbon resin, containing a silver halide (AgBr/AgCl) infrared fiber, allows convenient and reproducible loading of organic solutions and solids (amorphous or crystalline) derived by evaporation of the solvent. Attenuated total internal reflectance (ATR) measurements with a Fourier transform infrared (FT-IR) spectrometer are reported for organic compounds. Known spectroscopic features can be recognized with quantities as small as 6 ng (ca. $^1/_{20}$th of a monolayer). Usable spectra are obtainable with 100-ng quantities (1 monolayer), and high-quality spectra are measurable with 10-μg quantities. Absorbance is linear up to ca. 600 monolayers (0.55-μm layer thickness), the limit of absorption being ca. 0.9-μm layer thickness (about 1000 molecular layers).**

Infrared absorption spectra are useful for obtaining structural information about organic compounds. Substantial concentrations of material are normally used with suitable path lengths to compensate for the low absorption coefficients in the infrared region. Polar solvents require the use of special cell materials (usually expensive) and often have absorption bands in interesting regions. These difficulties may be overcome by the measurement of spectra of thin-layer films (*1*, *2*) by using attenuated total reflection (ATR) (*3*), but the currently available cells utilize costly crystals (ZnSe, Si, Ge, KRS-5, for example) and may not be convenient for samples with unusual physical characteristics. We recently reported the development of a silver halide (AgBr/AgCl) infrared fiber-optic cell for aqueous solutions (*4*). A different design was introduced for protein solutions and suspensions (*5*). We now describe a moderate-cost cell suitable for a variety of infrared measurements with organic materials; of especial interest are measurements on small amounts of solid deposited on the fiber by evaporation of a solution.

## EXPERIMENTAL SECTION

A specially designed cell (Figure 1) was used to measure spectra with a Nicolet 5DX Fourier transform infrared (FT-IR) spectrometer. The cell contains a 0.9-mm silver bromide/silver chloride polycrystalline fiber of 100-mm length, sealed into a Teflon-lined well with solvent-resistant gaskets. In our experiments, the FT-IR source radiation was focused on the input end of the infrared fiber with a ZnSe lens (25-mm focal length, 25-mm diameter). The radiation was collected from the exit of the fiber and collimated with a similar ZnSe lens. It was then introduced into the detector section of the FT-IR spectrometer, which incorporates a pyroelectric detector (deuteriated triglycine sulfate).

The silver halide fibers are fabricated by extruding a pure crystalline mixture of $AgCl_xBr_{1-x}$, with $x$ between 0.5 and 0.95, through a die at a temperature close to the softening point of the halide (*6-9*). The fiber inside the cell is readily removed and replaced. Exposure of the fiber to strong fluorescent or UV light should be avoided due to darkening. However, no noticeable degradation of fiber transmission was observed after prolonged exposure to incandescent lamp light or infrared radiation.

With a mount, the cell (illustrated in Figure 1) can be removed and replaced without affecting optical alignment. Solvent or solution may thus be introduced into the cell at locations away from the FT-IR spectrometer, a precaution necessary for avoiding contamination of the light path with solvent vapors.

After a background spectrum is measured with the clean fiber, about 250 μL of solvent is introduced into the cell, covering the fiber. The spectrum of the solvent is then measured. The solvent is removed, a solution of sample is introduced, and a spectrum is measured. The difference between the spectra is the spectrum of the sample in solution. The solvent may then be carefully evaporated with a gentle stream of dry nitrogen, leaving a thin solid film on the fiber, and the spectrum of the solid sample may now be measured. About 5 min (300 scans) is required for each spectrum of small amounts of material, but only 50 scans (less

0003-2700/88/0360-1908$01.50/0 